Applied Catalysis B: Environmental 164 (2015) 279–287

Contents lists available at ScienceDirect

Applied Catalysis B: Environmental

journal homepage: www.elsevier.com/locate/apcatb

Photocatalytic degradation and mineralization mechanism and toxicity assessment of antivirus drug acyclovir: Experimental and theoretical studies

Taicheng An[a,*], Jibin An[a,c], Yanpeng Gao[a,c], Guiying Li[a], Hansun Fang[a], Weihua Song[b]

[a] State Key Laboratory of Organic Geochemistry and Guangdong Key Laboratory of Environmental Protection and Resources Utilization, Guangzhou Institute of Geochemistry, Chinese Academy of Sciences, Guangzhou 510640, China
[b] Department of Environmental Science & Engineering, Fudan University, Shanghai 200433, China
[c] University of Chinese Academy of Sciences, Beijing 100049, China

ARTICLE INFO

Article history:
Received 5 August 2014
Accepted 6 September 2014
Available online 16 September 2014

Keywords:
Photocatalytic degradation
Antiviral drug
Degradation mechanism
Eco-toxicity evolution
Theoretical calculation

ABSTRACT

The degradation and mineralization of an antivirus drug acyclovir was attempted by using heterogeneous photocatalytic technology, and the high reactive •OH was found to be dominantly responsible for the degradation of acyclovir. Thus the frontier electron densities (FEDs) calculation was conducted to predict potential initial sites during the photocatalytic degradation, and the results found that •OH additions at C8 and C5, and H abstraction at C15, were found to be the three predominant degradation routes for •OH initiating degradation of acyclovir. Furthermore, the detail degradation mechanisms were also investigated by experimentally identified six major products using HPLC/MS/MS, and the formation possibility of three important products was also calculated to further validate the photocatalytic degradation mechanism with the quantum chemical calculations approach. In addition, to double confirm the proposed degradation mechanism, the corresponding kinetic models were proposed to explore acyclovir elimination and the formation of one main product (guanine) over the time profiles. Finally, the potential risk assessment results indicated that the aquatic toxicities at three trophic levels first increased and then decreased rapidly as the total organic carbon decreased.

© 2014 Elsevier B.V. All rights reserved.

1. Introduction

Pharmaceuticals and personal care products (PPCPs) are considered as emerging organic contaminates (EOCs) because they are frequently detected in surface waters and have potential impacts on both human health and ecological safety [1–3]. Pharmaceuticals are biologically active substances designed to cure diseases or prevent the spread of diseases. They are partially excreted from the body either as metabolites or as unchanged parent compounds into the aquatic environment [4]. These EOCs are usually not effectively eliminated by conventional sewage treatment plants. Once they are released in the aquatic environments, the biodegradation or photochemical degradation of these substances is insignificant, because some pharmaceutical residues have antibiotic activities or only present weak sunlight absorption [5]. In a consequence, the continuous discharge and accumulation of PPCPs into aqueous environments lead to their pseudo-persistence [6–9]. Although their concentrations in aquatic environments may be at trace levels, the adverse effects still can be harmful to the aquatic ecosystems as well as the public health [10–13].

These kinds of environmental impacts have been concerned about acyclovir, an effective antiviral drug used to treat the herpes virus [14]. This compound has poor bioavailability (only 10–20%), and is mainly excreted unchanged in urine when people taken orally, leading to at least ng L^{-1} level of this drug residue in water [15]. However, limited research can be found about the environmental fate of antiviral drugs, including acyclovir. Only two studies reported to investigate the biotransformation and ozonation of acyclovir [16,17]. Their researches found that the biodegradation half-life of acyclovir was only 5.3 h, indicating its rapid degradation during the conventional sewage treatment. However, a biorefractory product carboxy-acyclovir was identified during their biodegradation process, and could not be effectively removed even after 29 days treatment with activated sludge. Although this biorefractory product could be degraded by ozone and revealed no acute toxic effects on the microorganism (*Vibrio fischeri*), another

* Corresponding author. Tel.: +86 20 85291501; fax: +86 20 85290706.
E-mail address: antc99@gig.ac.cn (T. An).

http://dx.doi.org/10.1016/j.apcatb.2014.09.009
0926-3373/© 2014 Elsevier B.V. All rights reserved.

toxic degradation product (*N*-(4-carbamoyl-2-5-oxoimidazolidin)-formamido-*N*-methoxyacetic acid) was also subsequently formed. Thus, an alternative technology should be developed to detoxify this refractory compound, and also further research should be conducted to probe the transformation mechanisms as well as the fate of these emerging organic contaminants in aquatic environments.

End-of-pipe technologies, like advanced oxidation processes, are indispensable in reducing pharmaceuticals input into the aqueous environment. TiO_2 heterogeneous photocatalysis with highly reactive •OH has been proved to be a promising advanced oxidation technology to eliminate refractory organics in water [18,19], and the photocatalytic degradation of some model pharmaceuticals have been well studied [20,21]. The photocatalytic degradation of pharmaceuticals has mainly focused on the elimination kinetics and mechanisms of the parent compounds [22,23]. Nevertheless, some degradation products were identified to be more harmful to ecosystems and public health than their parental compounds [24], without consideration their mineralization [25]. Consequently, the identification of degradation products, the investigation of photocatalytic degradation mechanism and the assessment of their possible adverse effects on aquatic environments are all vital issue during the photocatalytic degradation these EOCs, though their concentrations are extremely low, and the synergistic or antagonistic effects may occur in degradation mixtures [26].

Exact identification of degradation products is a highly challenging task, due to unknown chemical structures, unavailable authentic standards, low concentrations and fast transformation of the intermediates. As such, quantum chemical calculation was recently employed to assist to explore the degradation mechanisms [21,27]. The insights into detailed mechanisms and the complement experimental studies are matched very well [28]. Unfortunately, very limited theoretical studies can be found on the •OH mediated degradation mechanisms of PPCPs during the photocatalytic degradation process, and even fewer works examined the fate and the toxicity assessment of PPCPs and their degradation intermediates [27,29].

In this study, the photocatalytic degradation kinetics and mechanism of an antiviral drug, acyclovir, were systematically studied under UV irradiation. The optimization of the degradation and mineralization of acyclovir were conducted using central composite design (CCD) method. The photocatalytic degradation mechanism of acyclovir was predict to be via electron extraction and •OH radical attack based on the data both achieved from HPLC/MS/MS as well as the calculated frontier electron densities (FEDs) and the reaction energy barrier. Then, a reasonable photocatalytic degradation mechanism of acyclovir was proposed, and an appropriate kinetic mode was also employed to confirm the acyclovir elimination and the formation of one dominated intermediates. Finally, the aquatic toxicities of acyclovir as well as its degradation products were assessed in detail at three different trophic levels during the photocatalytic degradation process.

2. Experimental

2.1. Materials and reagents

TiO_2 (P25, Degussa AG, Germany) was used as the photocatalyst, and acyclovir and guanine (≥99% purity) were purchased from Tokyo Chemical Industry Co., Ltd. Other reagents were of analytical grade. *Ptotobacterium phosphoreum* were from the Institute of Soil Science, Chinese Academy of Sciences. *Selenastrum capricornutum* and monoclonal *Daphnia magna* were kindly provided by Prof. Xiangping Nie, Institute of Hydrobiology, Jinan University, China. High-performance liquid chromatography (HPLC) grade water was used to prepare all solutions. Methanol (HPLC grade), obtained from Sigma, was used as received.

2.2. Experimental design and data analysis

The chemometric approach was performed using a CCD method [21,30]. The detailed experimental design is illustrated in Table S1, and the analysis of experimental data was supported by Design-Expert free software (trail version 8, Stat-Ease, Inc., Minnesota, USA).

2.3. Photocatalytic experiments and toxicity assays

Photocatalytic degradation experiments were carried out in an open Pyrex reactor (150 mL) with a double-walled cooling-water jacket to keep the solution temperature constant (25 ± 1 °C) throughout the experiments. The light source is a high-pressure mercury lamp (GGZ-125, Shanghai Yaming Lighting, E_{max} = 365 nm) with a power consumption of 125 W, which parallels to the photocatalytic reactor. The UV intensity was adjusted to 0.38 mW/cm^2 and measured with an UV-irradiance meter (UV-A, Beijing Normal University). A 150 mL acyclovir solution (100 μM) and a set amount of TiO_2 were added to the reactor according to experimental design values. Prior to illumination, the suspension was stirred in the dark for 30 min to achieve an adsorption equilibrium. Then, the UV light was turned on, signaling the start of photocatalysis. At given time intervals, 3 mL acyclovir solution samples were collected and filtered through 0.22 μm Millipore filters to remove TiO_2 particles for further analysis.

The toxicities of the treated acyclovir solutions were evaluated at three trophic levels, *P. phosphoreum*, *S. capricornutum* and *D. magna*. For the toxicity bioassay with *P. phosphoreum*, the luminescence was determined using a Dxy-3 analyzer (Nanjing Kuake, China), and the toxicity was determined after 15 min incubation. The *S. capricornutum* bioassay was carried out according to the Organization for Economic Co-operation and Development (OECD) guidelines for alga growth inhibition test No. 201; the algal biomass at different exposure times was measured by manually counting cells under the microscope. The *D. magna* bioassay was carried out according to the OECD guideline for *D. magna* acute immobilization test No. 202. *D. magna* neonates (<24 h hold) were used in all toxicity assays, and 10 neonates per replicate were used for each treatment in Pyrex beakers containing 50 mL of the test solution. The toxicological endpoint was the immobilization after 24 and 48 h exposure to the treated acyclovir solutions, and the definition of immobilization is that daphnia are not able to swim within 15 s after gentle agitation of the test vessel (even if they can still move their antennae). All the degradation and toxicity assessment experiments were replicated in triplicate.

2.4. Analytical procedures

The concentrations of acyclovir were analyzed using an Agilent 1200 series HPLC system equipped with a Kromasil C18 column (250 mm × 4.6 mm, 5 μm particle size) and performed at 30 °C. The mobile phase was a mixture of 90% water and 10% methanol (by volume) at flow rate of 1 mL min^{-1}. The detection wavelength was set up as 254 nm and the injection volume was 20 μL.

The Agilent iron-trap mass spectrometer (MSD-Trap-XTC) coupled with the Agilent HPLC system (1200 Series) was employed to elucidate photocatalytic degradation product structures. Samples from the photocatalytic experiments were separated using the Kromasil C18 column (250 mm × 4.6 mm, 5 μm particle size) with mobile phases of 7% CH_3OH and 93% formic acid solution (5 mM) at a flow rate of 0.5 mL min^{-1}. The MS analysis was performed with electrospray ionization (ESI) interface in the positive ion mode with

a capillary voltage of 3500 V. The nebulizer was set at 50 psi and dry gas (N_2) flow was 10 L min^{-1}. The dry gas temperature and source temperature were set at 350 °C and 120 °C, respectively.

A Dionex ion chromatograph (ICS-900) equipped with a conductivity detector was used to determine the organic acids. The separation was done using an Ion-Pac AS23 anion column (4 mm × 250 mm, Dionex) with a mixture of sodium carbonate (1.7 mM)/sodium bicarbonate (1.8 mM) as eluent at a flow rate of 1.0 mL min^{-1}. Total organic carbon (TOC) contents of samples were measured with a Shimadzu TOC-5000 analyzer (catalytic oxidation on Pt at 680 °C). Triplicate analyses were performed for each sample.

2.5. Computational methods

All quantum chemical calculations were done using the Gaussian 03 program [31]. Stationary point geometries were optimized using the hybrid density functional B3LYP method with the 6-31G(d,p) basis set, B3LYP/6-31G(d,p). Harmonic vibrational frequencies were calculated at the same level to identify all stationary points as either minima (zero imaginary frequency) or transition states (TSs; only one imaginary frequency), and to provide the thermodynamic contributions to free energy. Intrinsic reaction coordinate calculations were conducted to confirm that each TS really connected the corresponding reactants with the products. Single point energies, including the solvent effect, were calculated using the B3LYP/6-311++g(d,p), based on the optimized structures described above. The conductive polarizable continuum model was used to assess the solvent effect [32].

The frontier electron densities (FEDs) of the highest occupied molecular orbital (HOMO) and the lowest unoccupied molecular orbital (LUMO) were also determined [33,34] to predict the initial attack position by reactive species. Values of ($FED^2_{HOMO} + FED^2_{LUMO}$) were used to predict the reaction sites for the •OH addition positions, and the point charges were used to predict the reaction sites for H atom abstraction by •OH.

3. Results and discussion

3.1. Photocatalytic kinetic models and optimization

In the controls, no obvious acyclovir loss was observed, indicating that the adsorption and photolysis were negligible, but the photocatalytic degradation of acyclovir proceeded quickly, with the rate constant (k) of 0.0201 min^{-1} and the half-life ($t_{1/2}$) of 34.5 min (Fig. S1). The kinetic parameters and optimization results for the photocatalytic degradation and mineralization of acyclovir under various conditions in the CCD experiment are illustrated in Table S2. Based on the CCD matrix results, two semi-empirical equations (Eqs. S1 and S2) were obtained to describe the degradation and mineralization kinetics respectively, in which consist of 15 statistically significant coefficients. The detail discussion and validation of kinetics models on the degradation and mineralization are performed and shown in Figs. S2, S3 and Table S3. It revealed that the models were adequate to represent both degradation and mineralization kinetics of acyclovir.

As shown in Fig. 1, the Pareto diagram analysis was used to calculate the percentage effect of each response factor to identify which variables and interactions are more significant [35]. Acyclovir concentration (28.69%), pH (17.39%) and light intensity (43.17%) were found to be three main contributors affecting the photocatalytic degradation process, while acyclovir concentration (56.65%) and light intensity (8.42%) played important roles in the photocatalytic mineralization. Moreover, the photocatalytic mineralization efficiency was also affected by an interrelated variable:

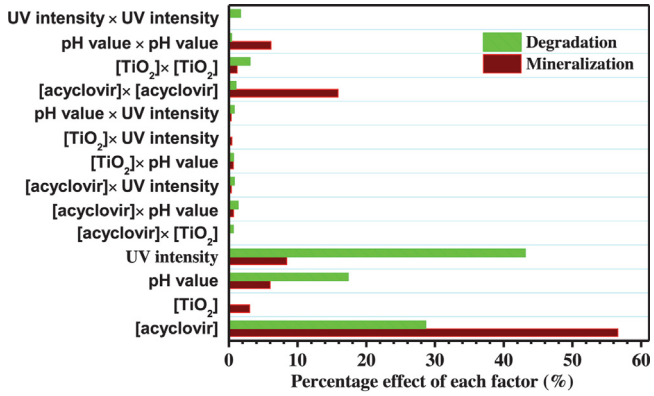

Fig. 1. Pareto graph for the photocatalytic degradation and mineralization efficiency of acyclovir.

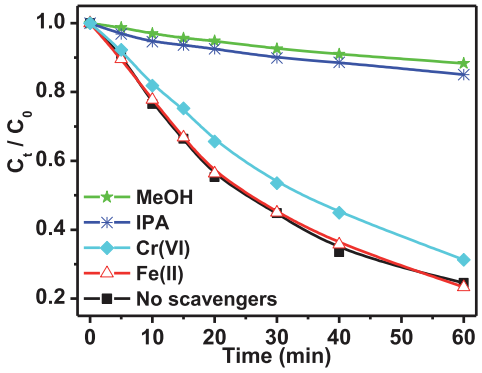

Fig. 2. The photocatalytic degradation kinetics of 100 μM acyclovir in presence of different reactive species scavengers with 0.1 M isopropanol, 0.1 M methanol, 50 μM $K_2Cr_2O_7$ and 10 μM Fe(II)-EDTA.

the two factor interactions of [acyclovir]^2, at 15.89%. Furthermore, contour plots for these significant variables were developed to optimize conditions for acyclovir degradation and mineralization (Fig. S4). Optimal conditions were optimized as 50 μM acyclovir concentration, 0.5 g L^{-1} TiO_2, pH value at 6.37 and 2.0 mW cm^{-2} light intensity, and the experimental degradation and mineralization efficiencies of acyclovir were obtained as 100% and 80.0%, respectively.

3.2. Photocatalytic mechanism

3.2.1. Contributions of different reactive species

It is generally accepted that the elimination of the organic compounds by TiO_2 photocatalysis can be attributed to the oxidation properties of photocatalytically generated reactive species (RSs), such as h^+, •OH, H_2O_2 and $O_2^{\bullet-}$ [36,37]. Nevertheless, the contribution of each RS was still unclear and dependent on the organics, as well as the system [23]. Therefore, different specific scavengers were used to investigate their indirect effects on the degradation efficiencies: isopropanol was used to scavenge •OH, methanol was for h^+ and •OH [38], $K_2Cr_2O_7$ was for e^- [39], and Fe(II)-EDTA was for H_2O_2 [29]. Fig. 2 shows the degradation kinetics with and without scavengers, and the corresponding pseudo-first-order rate constants under different conditions are also summarized in Table S4. The photocatalytic degradation rate constant was obtained as 0.0263 min^{-1} without scavengers, but it decreased to 0.0035 and 0.0031 min^{-1} with the addition of isopropanol or methanol, respectively, demonstrating the contribution of •OH and h^+ with 90.1% and 1.6%, respectively. Adding $K_2Cr_2O_7$ reduced the rate constant to 0.0213 min^{-1}, indicating that the valence band e^- was not

Table 1
Complete LC–MS/MS data for acyclovir and photocatalysis products.

No.	Retention time (min)	*m*/*z*	Structure	Main fragments MS^n (*m*/*z*)
0	23.2	226	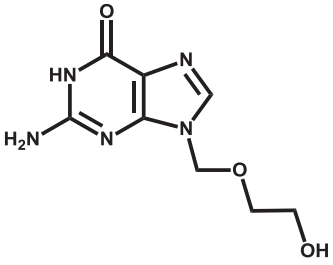	152 (MS^2 fragments of *m*/*z* 226)
1	21.6	242	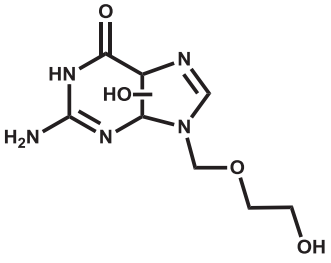	224, 152 (MS^2 fragments of *m*/*z* 242)
2	21.1	258	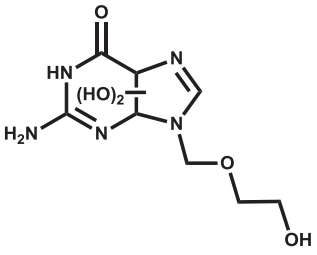	224, 208, 192 (MS^2 fragments of *m*/*z* 258)
3	5.5	186	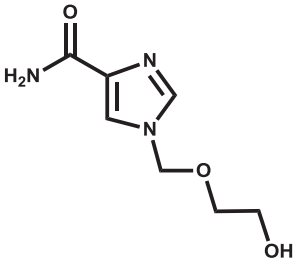	156, 141, 99 (MS^2 fragments of *m*/*z* 186); 125, 113 (MS^2 fragments of *m*/*z* 141 from *m*/*z* 186)
4	7.2	204	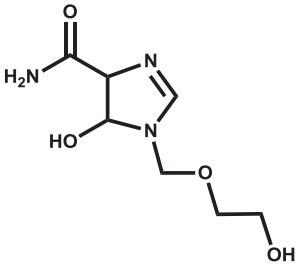	161, 143, 99, 60 (MS^2 fragments of *m*/*z* 204)
5	4.9	158	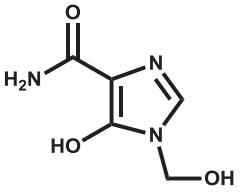	141, 115, 98, 86, 61 (MS^2 fragments of *m*/*z* 158)

Table 1 (*Continued*)

No.	Retention time (min)	*m*/*z*	Structure	Main fragments MS^n (*m*/*z*)
6	13.2	152	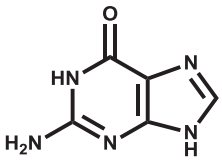	135, 110, 70 (MS^2 fragments of *m*/*z* 152)

important for acyclovir degradation in this photocatalytic system. The rate constant of 0.0262 min^{-1} did not substantially change in the presence of Fe(II)-EDTA, suggesting that H_2O_2 played a negligible role, or that a neglected amount of H_2O_2 was generated in this system. This result differed from the photocatalytic bacterial inactivation system previously reported by our group [40,41]. In brief, the high reactive •OH formed in the TiO_2 photocatalytic system was found to be major responsible for the photocatalytic degradation of acyclovir, but the valence band h^+ and the conductive band e^- were not highly involved in the degradation.

3.2.2. Photocatalytic degradation pathway

As discussed above, •OH was the major contributor to the photocatalytic degradation of acyclovir. Thus, the detailed degradation pathways as well as the degradation mechanisms were also attempted in the •OH mediated acyclovir oxidation. Further study using the HPLC/MS/MS revealed that six major products were formed during the degradation, as shown in Table 1. Retention times and detailed MS/MS data (such as molecule weight, structures, and fragmentation patterns) are summarized in Table S5. For example, the product 1 with *m*/*z* 242, corresponding to the addition of 16 mass units to the parent compound, was found to be consistent with monohydroxylated acyclovir. A daughter product, dihydroxylated acyclovir (product 2) with *m*/*z* 258 was also found. Both above-mentioned products showed shorter retention time than acyclovir due to increased polarity via the hydroxylation. The product 3 with *m*/*z* 186, product 4 with *m*/*z* 204 and product 5 with *m*/*z* 158 were also formed with the further cleavage of the isocytosine moiety from acyclovir molecule and identified with their fragmentation patterns. Another product with *m*/*z* 152 was also identified as guanine (product 6), which was validated by the fragmentation pattern of an authentic standard, and quantified during the photocatalytic degradation process.

To further elucidate the detailed reaction mechanisms of the •OH mediated photocatalytic degradation of acyclovir, quantum chemical calculations were performed to predict potential initial sites as well as the product formation processes. As reported by our previous studies, •OH usually oxidizes organics in aqueous media via three possible reaction mechanisms: •OH addition, H abstraction, and/or single electron transfer [42]. For the •OH addition pathways, •OH adducts were always the main products for the aromatic or unsaturation organics [21,43,44]; •OH might attack the aromatic ring or double bond of the organics, leading to form radical adduct. This further resulted in the production of hydroxylated products. Furthermore, the •OH attack sites can usually be predicted by the Frontier Orbital theory. That is, •OH radicals usually attack the sites with higher $FED^2_{HOMO} + FED^2_{LUMO}$ values [34,45].

The FEDs data of acyclovir molecule were calculated and summarized in Table 2. The results found C5 (0.42201), C7 (0.40579) and C8 (0.33637) atoms of acyclovir have higher $FED^2_{HOMO} + FED^2_{LUMO}$ values, indicating that these three positions are likely to be attacked by •OH through the •OH addition pathways. However, it remained unknown in which position happened. Therefore, the reaction energy (ΔG) and Gibbs free energy barrier ($\Delta G^{\neq}$) for these three pathways were calculated (Fig. 3a). The results found that all three pathways were exergonic processes ($\Delta G < 0$ kcal mol^{-1}), indicating that •OH addition to these three reaction sites might be thermodynamically favorable. The calculation data of the energy barrier further confirmed the possibility of these three kinds of addition pathways. When the •OH addition reaction took place at C7 or C8 atoms, the transient states of •OH adduct radical were formed, leading to the formation of the hydroxylated products with further radical oxidation. However, C8 is thought to be the precedential position mostly likely added by •OH, because it had lower reaction energy barrier than that of C7 (Fig. 3a). When the •OH addition reaction took place at the C5 atom, the transient state of •OH adduct radical was also formed first. With the further exothermic and lower (or no) reaction energy barrier of the oxidation process, the isocytosine moieties of the acyclovir molecule was ruptured and then formed a series of stable products.

The H abstraction pathway was also found to be significantly influencing the degradation products by the substituent groups. The electron withdrawing group could weaken the stability of the transition state, and the electric negative group in the molecule could lessen the H-abstraction constant by an order of magnitude [46]. Generally, the H abstraction reaction was likely to occur at atoms with a more positive charge. As shown in Table 2, C15 (0.14304) and C11 (0.25161) have showed more positive charge than other atoms. Therefore, both C15 and C11 atoms are the possible positions for the H abstraction reaction. Both pathways were found to be exergonic ($\Delta G < 0$ kcal mol^{-1}), indicating that H abstraction by •OH onto both reaction sites may be also thermodynamically favorable. However, the Gibbs free energy barrier ($\Delta G^{\neq}$) of the H abstraction at C15 was lower than C11 (Fig. 3b). Furthermore, more energy can be released from the reaction at the C15 position. Thus, C15 may be the precedential position for the H abstraction reaction to form acyclovir free radicals, with further exothermic and lower or no reaction energy barrier oxidation processes. Subsequently, the stable products with a ruptured side chain might be formed (Fig. 3b).

Table 2
Frontier electron densities and point charges on different atoms in acyclovir calculated using Gaussian 03 program at the B3LYP/6-31G* level.

Atom (number)	Point charge	$FED^2_{HOMO} + FED^2_{LUMO}$
C(1)	−0.10605	0.00250
C(2)	−0.11074	0.00373
O(3)	−0.74013	0.00091
N(4)	−0.77406	0.15406
C(5)	0.80644	0.42201
N(6)	−0.68545	0.12271
C(7)	0.45422	0.40579
C(8)	−0.12439	0.33637
C(9)	0.78100	0.02182
N(10)	−0.55761	0.12695
C(11)	0.25161	0.18426
N(12)	−0.46668	0.05217
O(13)	−0.62576	0.09704
N(14)	−0.90122	0.14224
C(15)	0.14304	0.01898
O(16)	−0.61523	0.02172

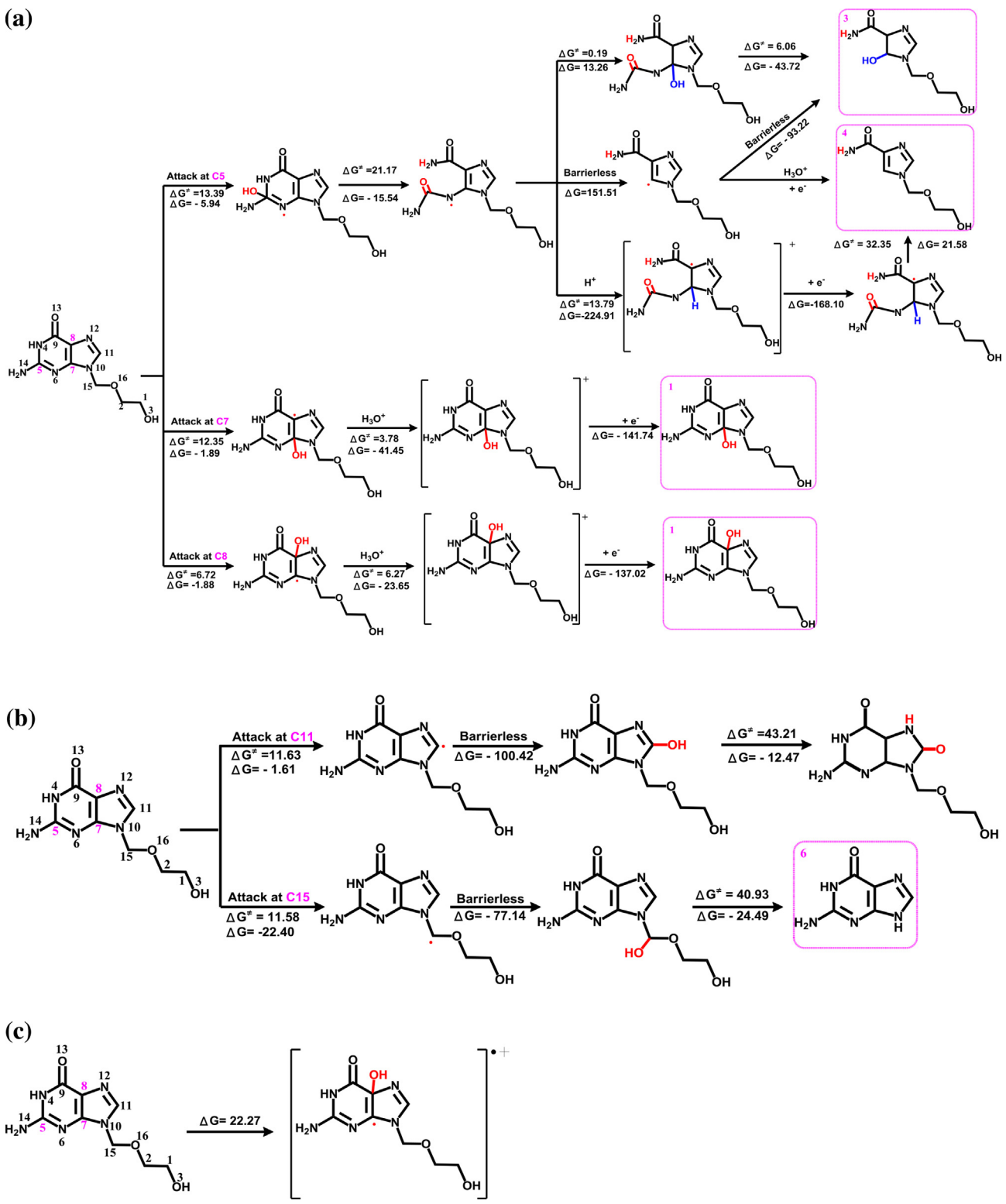

Fig. 3. Calculated •OH-addition (a), H-abstraction (b) and single electron transfer (c) routes in the initial reaction of acyclovir with •OH (The energy data are given in kcal mol^{-1}).

As similar report previously, electron transfer reactions generally barely contribute to the formation of products due to very short lived radical cations and the rapid hydrolysis to form •OH addition products [47]. Theoretical results (Fig. 3c) revealed a very high endothermic energy of 22.27 kcal mol^{-1} was obtained for the reaction with acyclovir. Thus, the single electron transfer pathway by •OH is confirmed as the impossible pathway and can be ignored in the photocatalytic degradation of acyclovir.

In summary, as discussed above, three predominant degradation pathways were proposed for •OH initiating degradation of acyclovir (Fig. 4). In pathway I, •OH reacted with acyclovir at C8 to form •OH-adduct, produced a hydroxylated products, such as

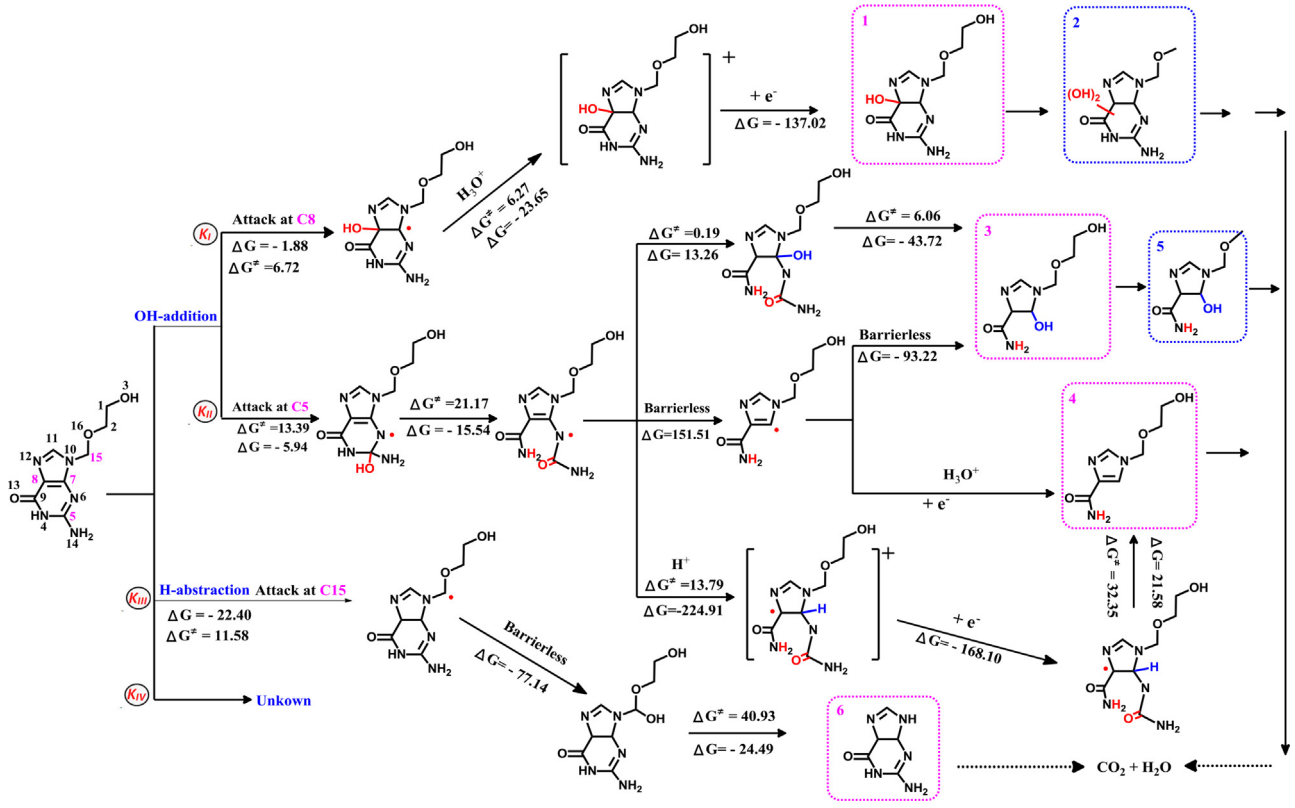

Fig. 4. Proposed photocatalytic degradation pathway of acyclovir (The energy data are given in kcal mol^{-1}).

monohydroxylated product 1 and dihydroxylated product 2. In pathway II, some cleavage products of the isocytosine moieties (such as products 3 and 4) were formed by •OH direct attack, and then were further oxidized to the daughter product 5. In pathway III, •OH attacks acyclovir through H abstraction at C15, resulting in the formation of product 6 (guanine). In all, acyclovir and formed products could be further completely mineralized into CO_2 and H_2O with prolonging the irradiation time with the photocatalytic technology.

Furthermore, the identified product 6, guanine, with the authentic standard was also used to confirm acyclovir elimination and guanine formation, and further validate the proposed photocatalytic degradation mechanism of acyclovir. Besides the three pathways above, the pathway IV was used to cover all uncertain degradation processes. Thus the total degradation kinetics are expressed as follows:

$$\frac{\mathrm{d[acyclovir]}}{\mathrm{d}t} = -(k_{\mathrm{I}} + k_{\mathrm{II}} + k_{\mathrm{III}} + k_{\mathrm{IV}})[\mathrm{acyclovir}] = -k_{\mathrm{app}}[\mathrm{acyclovir}] \quad (1)$$

where k_{I}, k_{II} and k_{III} are the rate constants for the three pathway in Fig. 4; k_{IV} is the rate constant of all uncertain processes; k_{app} is the overall apparent pseudo-first-order rate constant measured above in the kinetics section. Thus, the formation rate of guanine can be expressed as follows:

$$\frac{\mathrm{d[guanine]}}{\mathrm{d}t} = k_{\mathrm{III}}[\mathrm{acyclovir}] - k_g[\mathrm{guanine}] \quad (2)$$

where k_g is the overall rate constant for the photocatalytic degradation of guanine. As mentioned above, the photocatalytic degradation of acyclovir obeys pseudo-first-order kinetics. Therefore, by assuming that all the reactions involved in the above scheme obey pseudo-first-order kinetics, to make an indefinite integral of Eqs. (1) and (2) to give Eqs. (3) and (4):

$$C_{\mathrm{acyclovir}} = C^0_{\mathrm{acyclovir}} e^{-kt} \quad (3)$$

$$C_{\mathrm{guanine}} = \frac{C^0_{\mathrm{acyclovir}} k_{III}}{k_g - k}[e^{-kt} - e^{-k_g t}] \quad (4)$$

where $C^0_{\mathrm{acyclovir}}$ is the initial acyclovir concentration; C_{guanine} is the guanine concentration. Thus, these two equations can be used to predict acyclovir degradation and guanine formation concentrations as a function of time, further confirming the correctness of the proposed degradation mechanism. Eq. (3) expresses the concentration of acyclovir as a function of irradiation time, while Eq. (4) expresses the formation and further degradation of guanine during the photocatalytic process. The rate constant k is the degradation of acyclovir, and the rate constant k_{III} and k_g can be determined by fitting observed experimental data using Matlab 7.0 (Fig. 5). The results found that 98.6% of 100 μM acyclovir could be eliminated

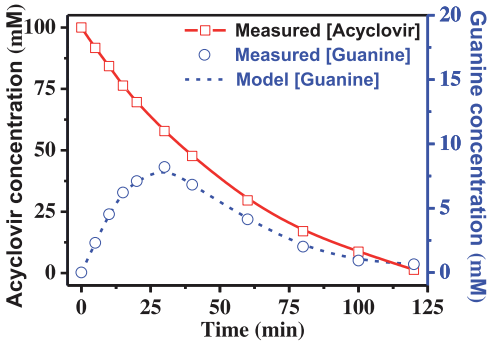

Fig. 5. Mathematical model of photocatalytic elimination of acyclovir and the formation of guanine.

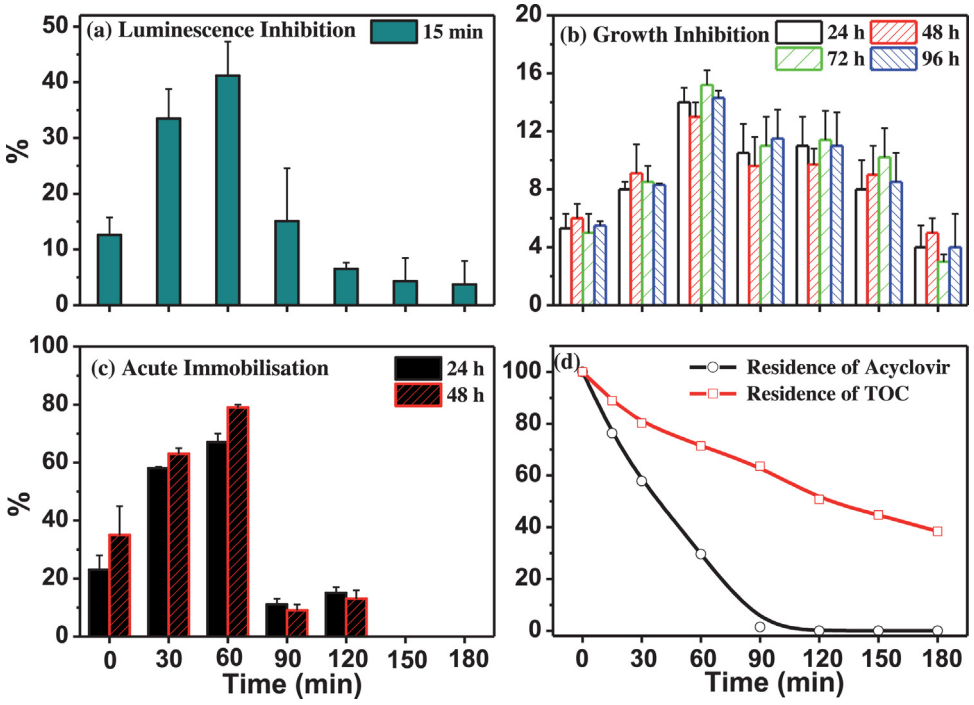

Fig. 6. Evolution of acute toxicity evaluated with (a) *Photobacterium phosphoreum*, (b) *Selenastrum capricornutum*, and (c) *Daphnia magna*, and (d) both TOC reduction and acyclovir residues during the photocatalytic degradation of acyclovir.

within 120 min, and 30.8% (calculated form k_{III}/k_{app}) of acyclovir was transformed into guanine by pathway III. Through this way, H abstraction is confirmed to be a relatively important pathway for the •OH mediated photocatalytic degradation of acyclovir in water. Of course, other pathways totally contributed to around 69.2%.

3.3. Aquatic toxicity assessments

As discussed above, it can be concluded that the TiO_2 photocatalytic process with highly reactive •OH could effectively eliminate acyclovir, and a complex products were also produced. To further investigate the potential risk of this pharmaceuticals as well as its degradation products, to aquatic organisms, the acute toxicities evolution at three trophic levels species were also performed before and after treatment. In this work, the aquatic toxicities were assessed at different irradiation intervals using a 100 μM acyclovir solution with three trophic level species, *P. phosphoreum* (15 min), *S. capricornutum* (96 h) and *D. magna* (48 h). As shown in Fig. 6, three species were found to be inhibited with 12.3%, 4.8%, and 35.1% upon 100 μM acyclovir solution exposure, respectively. As the degradation proceeded, the residual acyclovir concentration decreased rapidly, but the eco-toxicities of the treated solutions toward three level species all increased gradually, with inhibition efficiencies of 41.2%, 14.3%, and 79.0% with increasing irradiation time up to 60 min. It implies that more toxic products were produced during the photocatalytic degradation of acyclovir. When 100% of acyclovir was eliminated within 120 min, the inhibition efficiencies of the treated solution remained at 7.2%, 10.8%, and 14.4% for *P. phosphoreum* (15 min), *S. capricornutum* (96 h), and *D. magna* (48 h), respectively. However, with further irradiation, the toxic products could be eliminated and the acute toxicity of treated solutions decreased significantly as TOC reduction, although the final treated solution still had a weak inhibition effect on these aquatic organisms. In summary, acyclovir degradation with TiO_2 photocatalysis can be accomplished successfully, but the products were found to be more harmful to aquatic organisms. Thus, for safe water treatment, the treatment duration should be carefully selected to completely decontaminate acyclovir and totally reduce the acute eco-toxicity of treated solutions with different employed advanced oxidation technologies for example the heterogeneous photocatalysis.

4. Conclusion

A full picture of the photocatalytic degradation and mineralization of acyclovir was investigated using CCD, and two semi-empirical expressions were obtained and successfully used to model both processes. The products identification revealed that •OH addition and H abstraction routes are major •OH mediated pathways. And the computational approach to predict potential initial sites as well as the product formation processes is found to be a cost-effective way to propose the photocatalytic degradation mechanisms of EOCs, for example antiviral drug acyclovir, with assistant with the experimental MS spectra results. Additionally, the toxicity assessment of the photocatalytically treated solutions showed that the TiO_2 photocatalytic process is an efficient technology to reduce the toxicity of acyclovir solutions, although this process needs sufficient irradiation time to completely decontaminate generated products. Our results herein demonstrate that advanced oxidation technologies for example heterogeneous photocatalytic process are very effective, and are promising technologies to detoxify EOCs, as well as their degraded toxic products.

Acknowledgments

This is contribution No. IS-1956 from GIGCAS. The authors appreciate the financial supports from National Natural Science Foundation of China (40973068), Knowledge Innovation Program of CAS (KZCX2-YW-QN103), Science and Technology Project of Guangdong Province, China (2012A032300010) and Earmarked Fund of SKLOG (SKLOG2011A02).

Appendix A. Supplementary data

Supplementary data associated with this article can be found, in the online version, at http://dx.doi.org/10.1016/j.apcatb.2014.09.009.

References

[1] S.K. Khetan, T.J. Collins, Chem. Rev. 107 (2007) 2319–2364.
[2] R.P. Schwarzenbach, B.I. Escher, K. Fenner, T.B. Hofstetter, C.A. Johnson, U. von Gunten, B. Wehrli, Science 313 (2006) 1072–1077.
[3] C.G. Daughton, T.A. Ternes, Environ. Health Perspect. 107 (1999) 907–938.
[4] S.E. Jorgensen, B. Halling-Sorensen, Chemosphere 40 (2000) 691–699.
[5] K. Ikehata, N. Jodeiri Naghashkar, M. Gamal El-Din, Ozone Sci. Eng. 28 (2006) 353–414.
[6] S. Suarez, M. Carballa, F. Omil, J.M. Lema, Rev. Environ. Sci. Bio/Technol. 7 (2008) 125–138.
[7] W. Xue, C. Wu, K. Xiao, X. Huang, H. Zhou, H. Tsuno, H. Tanaka, Water Res. 44 (2010) 5999–6010.
[8] E. Walters, K. McClellan, R.U. Halden, Water Res. 44 (2010) 6011–6020.
[9] R.L. Oulton, T. Kohn, D.M. Cwiertny, J. Environ. Monit. 12 (2010) 1956–1978.
[10] B. Halling-Sørensen, S. Nors Nielsen, P.F. Lanzky, F. Ingerslev, H.C. Holten Lützhøft, S.E. Jørgensen, Chemosphere 36 (1998) 357–393.
[11] L. Guardabassi, D.M.A. Lo Fo Wong, A. Dalsgaard, Water Res. 36 (2002) 1955–1964.
[12] E.F. Orlando, A.S. Kolok, G.A. Binzcik, J.L. Gates, M.K. Horton, C.S. Lambright, L.E. Gray, A.M. Soto, L.J. Guillette, Environ. Health Perspect. 112 (2004) 353–358.
[13] M. Cleuvers, Chemosphere 59 (2005) 199–205.
[14] S.D. Brown, C.A. White, C.K. Chu, M.G. Bartlett, J. Chromatogr. B 772 (2002) 327–334.
[15] C. Prasse, M.P. Schlusener, R. Schulz, T.A. Ternes, Environ. Sci. Technol. 44 (2010) 1728–1735.
[16] C. Prasse, M. Wagner, R. Schulz, T.A. Ternes, Environ. Sci. Technol. 46 (2012) 2169–2178.
[17] C. Prasse, M. Wagner, R. Schulz, T.A. Ternes, Environ. Sci. Technol. 45 (2011) 2761–2769.
[18] T.C. An, H. Yang, W.H. Song, G.Y. Li, H.Y. Luo, W.J. Cooper, J. Phys. Chem. A 114 (2010) 2569–2575.
[19] M. Klavarioti, D. Mantzavinos, D. Kassinos, Environ. Int. 35 (2009) 402–417.
[20] S. Yurdakal, V. Loddo, V. Augugliaro, H. Berber, G. Palmisano, L. Palmisano, Catal. Today 129 (2007) 9–15.
[21] T.C. An, J.B. An, H. Yang, G.Y. Li, H.X. Feng, X.P. Nie, J. Hazard. Mater. 197 (2011) 229–236.
[22] V.A. Sakkas, P. Calza, C. Medana, A.E. Villioti, C. Baiocchi, E. Pelizzetti, T. Albanis, Appl. Catal. B: Environ. 77 (2007) 135–144.
[23] H. Yang, T.C. An, G.Y. Li, W.H. Song, W.J. Cooper, H.Y. Luo, X.D. Guo, J. Hazard. Mater. 179 (2010) 834–839.
[24] D. Vogna, R. Marotta, R. Andreozzi, A. Napolitano, M. d'Ischia, Chemosphere 54 (2004) 497–505.
[25] T.E. Doll, F.H. Frimmel, Water Res. 38 (2004) 955–964.
[26] M. la Farre, S. Perez, L. Kantiani, D. Barcelo, Trac-Trend Anal. Chem. 27 (2008) 991–1007.
[27] Y.P. Gao, Y.M. Ji, G.Y. Li, T.C. An, Water Res. 49 (2014) 360–370.
[28] D. Minakata, W. Song, J. Crittenden, Environ. Sci. Technol. 45 (2011) 6057–6065.
[29] H.S. Fang, Y.P. Gao, G.Y. Li, J.B. An, P.K. Wong, H.Y. Fu, S.D. Yao, X.P. Nie, T.C. An, Environ. Sci. Technol. 47 (2013) 2704–2712.
[30] V.A. Sakkas, M.A. Islam, C. Stalikas, T.A. Albanis, J. Hazard. Mater. 175 (2010) 33–44.
[31] M.J. Frisch, G.W. Truck, H.B. Schlegel, G.E. Scuseria, M.A. Robb, J.R. Cheeseman, V.G. Zakrzewski, J.A. Montgomery, J.R.E. Stratmann, J.C. Burant, S. Dapprich, J.M. Millam, A.D. Daniels, K.N. Kudin, M.C. Strain, O. Farkas, J. Tomasi, V. Barone, M. Cossi, R. Cammi, B. Mennucci, C. Pomelli, C. Adamo, S. Clifford, J. Ochterski, G.A. Petersson, P.Y. Ayala, Q. Cui, K. Morokuma, D.K. Malick, A.D. Rabuck, K. Raghavachari, J.B. Foresman, J. Cioslowski, J.V. Ortiz, A.G. Boboul, B.B. Stefnov, G. Liu, A. Liaschenko, P. Piskorz, L. Komaromi, R. Gomperts, R.L. Martin, D.J. Fox, T. Keith, M.A. Al-Laham, C.Y. Peng, A. Nanayakkara, C. Gonzalez, M. Challacombe, P.M.W. Gill, B. Johnson, W. Chen, M.W. Wong, J.L. Andres, C. Gonzalez, M. Head-Gordon, E.S. Replogle, J.A. Pople, GAUSSIAN 03, Guassian Inc., Pittsburgh, PA, 2003.
[32] V. Barone, M. Cossi, J. Phys. Chem. A 102 (1998) 1995–2001.
[33] T.C. An, H. Yang, G.Y. Li, W.H. Song, W.J. Cooper, X.P. Nie, Appl. Catal. B-Environ. 94 (2010) 288–294.
[34] K. Fukui, T. Yonezawa, H. Shingu, J. Chem. Phys. 20 (1952) 722–725.
[35] A.K. Abdessalem, N. Oturan, N. Bellakhal, M. Dachraoui, M.A. Oturan, Appl. Catal. B: Environ. 78 (2008) 334–341.
[36] L. Yang, L.E. Yu, M.B. Ray, Water Res. 42 (2008) 3480–3488.
[37] M.N. Chong, B. Jin, C.W.K. Chow, C. Saint, Water Res. 44 (2010) 2997–3027.
[38] A.L. Teel, C.R. Warberg, D.A. Atkinson, R.J. Watts, Water Res. 35 (2001) 977–984.
[39] Y. Chen, S. Yang, K. Wang, L. Lou, J. Photochem. Photobiol. A 172 (2005) 47–54.
[40] W. Wang, T.W. Ng, W.K. Ho, J. Huang, S. Liang, T. An, G. Li, J.C. Yu, P.K. Wong, Appl. Catal. B: Environ. 129 (2013) 482–490.
[41] Y.M. Chen, A.H. Lu, Y. Li, L.S. Zhang, H.Y. Yip, H.J. Zhao, T.C. An, P.K. Wong, Environ. Sci. Technol. 45 (2011) 5689–5695.
[42] T.C. An, Y.P. Gao, G.Y. Li, P.V. Kamat, J. Peller, M.V. Joyce, Environ. Sci. Technol. 48 (2014) 641–648.
[43] V. Brezová, M. Čeppan, E. Brandšteterová, M. Breza, L. Lapčík, J. Photochem. Photobiol. A 59 (1991) 385–391.
[44] T.D. Bui, A. Kimura, S. Ikeda, M. Matsumura, J. Am. Chem. Soc. 132 (2010) 8453–8458.
[45] T.C. An, L. Sun, G.Y. Li, Y.P. Gao, G.G. Ying, Appl. Catal. B: Environ. 102 (2011) 140–146.
[46] S. Mitroka, S. Zimmeck, D. Troya, J.M. Tanko, J. Am. Chem. Soc. 132 (2010) 2907–2913.
[47] A.R. Nicolaescu, O. Wiest, P.V. Kamat, J. Phys. Chem. A 107 (2003) 427–433.